Manipulating Surface Plasmon Polaritons Using F-Shaped Nanoslits Array

Liang Cao, Wenting Li, Yongkai Wang, Xiaojun Tian, Guian Li, Hairong Zheng, and Zhongyue Zhang

***Abstract*— F-shaped nanoslits were arranged linearly and circularly to manipulate surface plasmon polaritons (SPPs) using circular polarization illumination. Numerical calculations show that when F-shaped nanoslits are linearly arranged, the electric field distribution follows unidirectional stripe-shaped patterns. Focusing is observed with a circular arrangement of the nanoslits under circular polarization illumination with specific handedness. For the latter geometry, electric fields are greatly enhanced and converge to inside the circle. These results are relevant for the design of nanophotonic devices with applications sensitive to polarization, focusing SPPs, and generating large electric fields.**

***Index Terms*— Finite element method, plasmonics, surface plasmon polaritons.**

I. Introduction

With the development of nanofabrication and microelectronics technologies, plasmonics has increasingly attracted the attention of researchers over the past several decades. When light illuminate a noble metal surface and excites the collective oscillation of electrons localized at the surface, the surface electron density wave and coupled electromagnetic wave are generated, which is known as surface plasmon polaritons (SPPs) [1]. Given that SPPs in metals and dielectric layer exponentially decay, the diffraction limit can be surpassed [2], thereby enabling applications in nanolithography [3], [4], nanoresolution optical imaging techniques [5], and enhanced transmission [6] feasible.

Extreme light concentration shows great application potential in ultrafast photodetectors, higher-efficiency solar cells, locally controlled catalysis, and thermally stimulated processes [7]–[11]. The electric field distribution on the metal surface can be controlled by manipulating the SPPs. Researchers have designed various structures to control the propagation of SPPs or the distribution of electric fields. For the linear polarization illumination model, because of the same excited phase throughout its whole structure, structural geometry plays the key role in manipulating SPPs. Recently, dielectric Fresnel zone plates [12], [13], curved slits on the metal surface [14]–[16], a single subwavelength metal slit surrounded by chirped dielectric surface gratings [17], and metallic nanoslits with variant widths [18] have been used to focus the SPPs. However, for the circular polarization illumination model, structural geometrical features must be improved to match the excited phases because SPPs can only be generated only when the incident light polarization is perpendicular to the slit [19]. From then on, the geometric phase effect of the archimedean spiral slit has been used to focuse SPPs at irradiations with the left-hand and right-hand circular polarizations into spatially separated plasmonic fields [20], thereby generating circularly polarized vortex emission [21], [22], and miniaturizing the circular polarization analyzer [23]–[25]. Recently, nanostructures composed of subwavelength apertures have been designed to tune SPPs excited by light with circular polarization [19]. The SPP emission pattern of a subwavelength aperture is approximately the same as that of an in-plane dipole. Researchers have arranged many of these short perpendicular slits in a column, and the interference effect of these dipoles have resulted in the polarization-controlled tunable directional coupling of SPPs at different illumination polarizations.

In this letter, F-shaped slits array are used to manipulate SPPs. The F, which consists of two horizontal lines and one vertical line, is a simple chiral structure. Under left-handed circular polarization (LCP) and right-handed circular polarization (RCP) illuminations, the in-plane scattering properties of the F-shaped slit are different. The finite element method is used to simulate electric field distributions at the metal surface. Results show that the F-shaped slit array generates different electric field distributional patterns (EFDPs) on two sides of the F-shaped slit array through the circular polarization illumination. A reversed EFDP appears when the handedness of the circular polarization is changed. When the F-shaped slit array is bent into a circle, the handedness of the circular polarization of illumination changes the electric field distribution inside the circle. These results enrich the components of nanophotonic devices to analyze the circular polarization, focusing SPPs, and generating large electric fields.

II. Structure and Method

Figure 1 shows the F-shaped slit array in two mirror-symmetric columns. As shown in Fig. 1, the distance between the centers of the two columns is S. The spaces between adjacent F-shaped slits in both columns are H. For an individual

Manuscript received February 25, 2014; revised April 10, 2014; accepted April 20, 2014. Date of publication April 23, 2014; date of current version May 22, 2014. This work was supported in part by the National Natural Science Foundation of China under Grant 11004160, in part by the Fundamental Research Funds for the Central Universities under Grant GK201303007, and in part by the Funds for Undergraduate Students Innovation Training under Grant 201310718035.

The authors are with the School of Physics and Information Technology, Shaanxi Normal University, Xi'an 710062, China (e-mail: caolianger2011@gmail.com; 631336819@qq.com; wang_yong_kai@126.com; tianxiaojun@snnu.edu.cn; liguian@snnu.edu.cn; hrzheng@snnu.edu.cn; zyzhang@snnu.edu.cn).

Color versions of one or more of the figures in this letter are available online at http://ieeexplore.ieee.org.

Digital Object Identifier 10.1109/LPT.2014.2319354

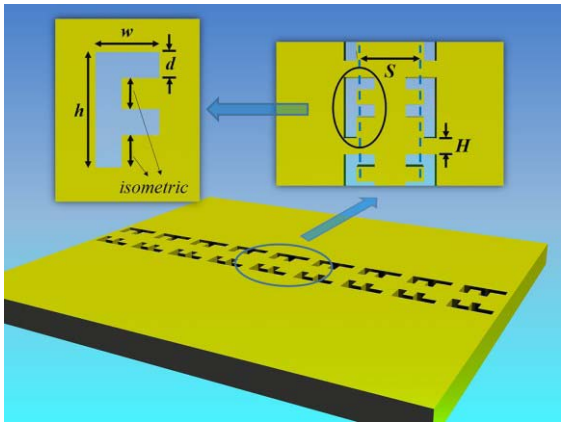

Fig. 1. F-shaped slits array consisting of two mirror-symmetric columns and the structural parameters of F-shaped slits array.

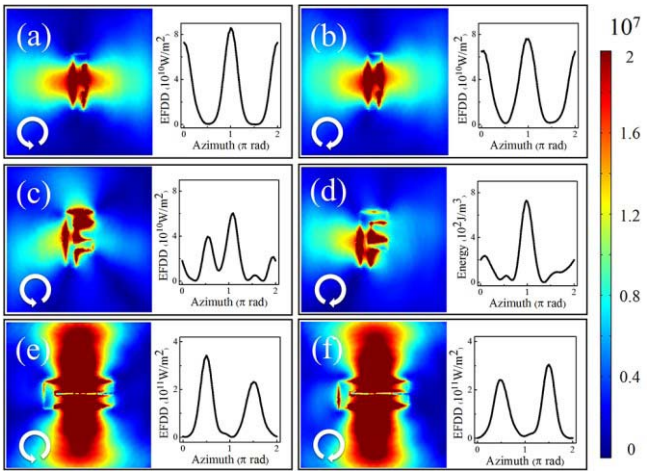

Fig. 2. EFDPs and EFDDs of F-shaped slits array with specific parameters at LCP and RCP illuminations: (a), (b) $w = \lambda_{SPPs}/4$ and $h = \lambda_{SPPs}$; (c), (d) $w = \lambda_{SPPs}/2$ and $h = \lambda_{SPPs}$; (e), (f) $w = \lambda_{SPPs}$ and $h = \lambda_{SPPs}/2$.

F-shaped slit, the width of the slit is d. The height and the width of the "F" are represented by h and w, respectively. The distance from the upper branch to the middle branch and the distance from the middle branch to the bottom of "F" are identical. The F-shaped slits are built in 300 nm-thick gold film.

The finite element method (COMSOL Multiphysics) is used to simulate EFDP. The periodic conditions are set at the left and right boundaries, and the perfectly matched layers are set at the front and back boundaries. Thus, the gold film can be considered to have infinite length. The structure is bottom illuminated (illuminated along the direction perpendicular to the surface of gold film) by circular polarized light at a wavelength of 532 nm. At this wavelength, the refractive index is $n_{\mathrm{Au}} = 0.467 + i\ 2.408$, and the wavelength of the SPPs at the gold film is $\lambda_{\mathrm{SPPs}} = 489$ nm. The magnitude of the incident electric field is set at 1 V/m.

III. Results and Discussion

Firstly, we investigate the in-plane emission property of a single F-shaped slit subjected to LCP and RCP illuminations. In this letter, the width w and the height h of the "F" are varied from $\lambda_{\mathrm{SPPs}}/4$ to $5\lambda_{\mathrm{SPPs}}/4$ and from $\lambda_{\mathrm{SPPs}}/2$ to $3\lambda_{\mathrm{SPPs}}/2$, respectively. The slit width d is 100 nm. Results show that the emission properties of the F-shaped slit strongly depend on its structural parameters. In addition to the EFDPs, the energy flow density distributions (EFDDs) at different azimuth angles are also investigated and the emission property of the F-shaped slit is revealed. Figure 2 shows the EFDPs and EFDDs of the three structures through circular polarization illumination at different handednesses. The structural parameters are $w = \lambda_{\mathrm{SPPs}}/4$ and $h = \lambda_{\mathrm{SPPs}}$ (Figs. 2a and 2b), $w = \lambda_{\mathrm{SPPs}}/2$ and $h = \lambda_{\mathrm{SPPs}}$ (Figs. 2c and 2d), and $w = \lambda_{\mathrm{SPPs}}$ and $h = \lambda_{\mathrm{SPPs}}/2$ (Figs. 2e and 2f). When the F-shape slit is narrow in either the vertical or horizontal direction, the EFDPs are bidirectionally launched (Figs. 2a, 2b, 2e, and 2f)). When the width w is comparable to h, the emissions of the SPPs are multidirectionally launched, and the EFDPs show difference at LCP and RCP illuminations (Figs. 2c and 2d). Additional results also show that when w is comparable to h, EFDPs strongly depend on the structural parameters of "F". The F-shaped slit consists of the left part, upper branch, and middle branch. Each part can be regarded as an in-plane dipole. When the F-shaped slit is narrow in the horizontal direction (smaller w), the emission effects of the upper and middle branch are negligible, and the entire F-shaped slit can be regarded as an in-plane dipole, which mainly launches SPPs to the left and right directions. Similarly, when an F-shaped slit is narrow in the vertical direction (smaller h), the entire F-shape slit can be regarded as two parallel dipoles, and the SPPs launch up and down. However, when w is comparable to h, the emission effects of all three parts are considerable. Given the phase delays between the emissions of the three parts, the EFDP is complicated and multidirectionally launched.

Considering that F-shaped slits with comparable w and h have different EFDPs at different circular polarization illuminations, the F-shaped slits arranged in different patterns accordingly generate different EFDPs. When F-shaped slits are arranged in two separate columns (Fig. 1), different EFDPs exist at the LCP and RCP illuminations (Figs. 3a and 3b). The structural parameters are $H = 130$ nm, $h = \lambda_{\mathrm{SPP}}$, and $d = 100$ nm. As shown in Fig. 3a, a stripe shaped EFDP exists on the left side of the F-shaped slit array, and a spot shaped EFDP exists on the right side through LCP illumination. As shown in Fig. 3b, a stripe shaped EFDP exists on the right side, and a spot shaped EFDP exists on the left side through RCP illumination. In comparison, the EFDP at linear polarization illumination is also calculated, and a spot shaped EFDP is found on two sides (Fig. 3c). The phase distribution of the out-plane component of the electric fields is calculated and shown in Figs. 3d-3f corresponding to the EFDPs of Figs. 3a-3c, respectively. The phase distributions are consistent with the EFDPs of Figs. 3a-3c.

The effects of H and S between adjacent "F" on the EFDP are further investigated. Figure 4b shows the electric field intensity subject to LCP illumination along line 1 in Fig. 4a which passes through the center of one "F". The electric fields

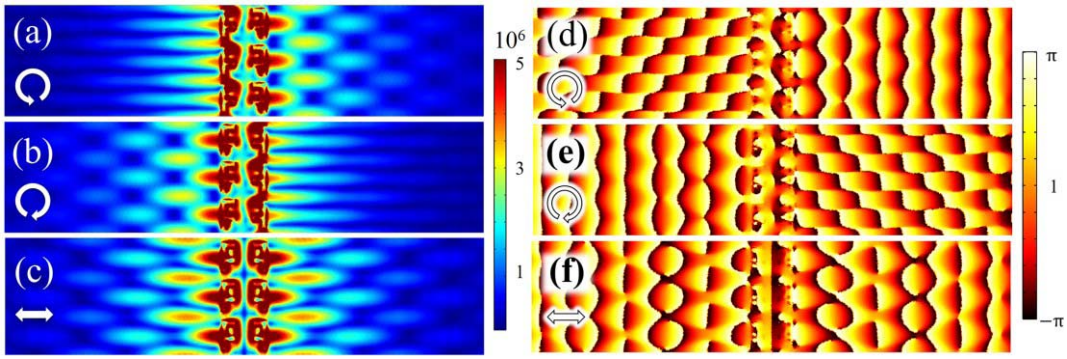

Fig. 3. EFDPs [(a)–(c)] and Phase distribution of out-plane component of SPPs [(d)–(f)] of F-shaped slits array at illuminations with different polarization: (a), (d) LCP; (b), (e) RCP; (c), (f) linear polarization.

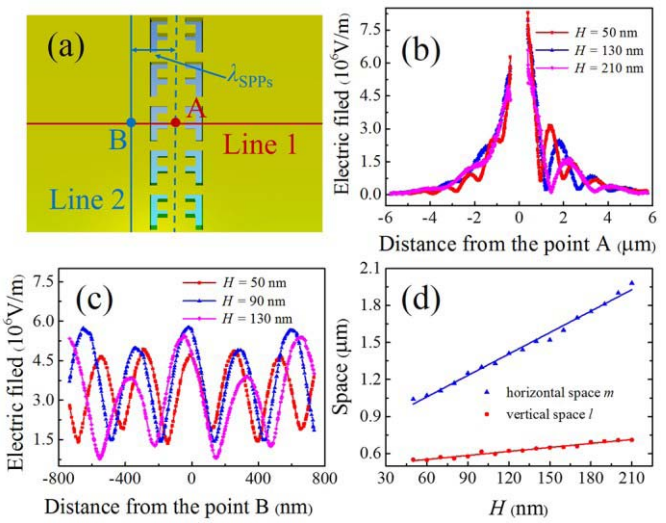

Fig. 4. (a) F-shaped slits array with line 1 and line 2; (b), (c) electric field intensities along line1 and line 2, respectively; (d) vertical and horizontal spaces between adjacent spots as a function of H.

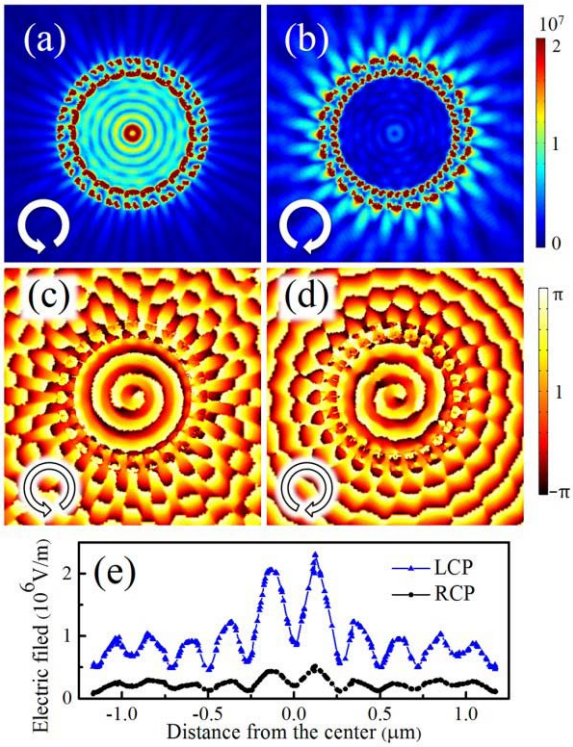

Fig. 5. EFDPs of the bent F-shaped slits array at LCP (a) and RCP (b) illuminations, respectively. Phase distribution of out-plane component of electric fields of the bent F-shaped slits array at LCP (c) and RCP (d) illuminations, respectively. (e) Electric field intensities along a diameter of the circle.

exponentially decay on the left side of the F-shaped slit arrays, and some peaks appear on the right side, consistent with the previous results shown in Fig. 3a. With increased H, the peaks shift away from the F-shaped slit arrays. Figure 4c shows the electric field intensity along line 2 in Fig. 4a, which is in the array direction and λ_{SPPs} away from the center of the F-shaped slit array, point B. Large electric fields periodically occur along line 2. With increased H, the period increases. Figure 4d shows the vertical space l and the horizontal space m between adjacent spots as a function of H. With increased H from 50 nm to 210 nm, l increases from ∼550 nm to ∼710 nm and m increases from ∼1040 nm to ∼1980 nm, respectively. The solid lines in Fig. 4d represent the linear fittings.

Figure 5a and 5b show the electric field distributions of the circularly arranged F-shaped slits arrays subjected to LCP and RCP illuminations, respectively. The structure parameters of a single F-shaped slit are $h = 300$ nm, $w = 150$ nm, and $d = 50$ nm. The separations between adjacent "F" are $S = \lambda_{SPPs}/2$ and $H \approx 130$ nm. The radius of the circle R is $3\lambda_{SPPs}$. As shown in Fig. 5a, with LCP illumination, the EFDP shows large electric fields that form concentric rings inside the circle. As shown in Fig. 5b, large electric fields appear outside the circle when the arrays are subjected to RCP illumination. Figure 5c shows the electric fields along one diameter of the circle. The electric field inside the circle under LCP illumination is approximately five times larger than that under RCP illumination. Under LCP illumination, 2.21% energy is scattered away from the center compared with the incident light on the area surrounded by an F-shaped slit array and 83.2% of these energy is scattered toward the center. Under RCP illumination, 4.39% energy is scattered away from the center compared with the incident

light, and only 5.5% of these energy is scattered toward the center. Thus, the bent F-shaped slit array provides another way to distinguish the circular polarizations of incident light. The phase distributions of the out-plane component of the electric fields in Figs. 5a and 5b are also calculated, as shown in Figs. 5c and 5d, respectively. Subjected to LCP and RCP illumination, the bent F-shaped slit array generates surface plasmon vortices with topologic charges of -1 and $+1$, respectively. These results are consistent with the single plasmon vortex lens possessing a zero geometric vortex topologic charge [26]. The topologic charge of our proposed F-shaped slit array arises from the geometric berry phase because of the interaction of circularly incident light with a circularly arranged nanoscale structure [27].

IV. Conclusion

The EFDPs of linearly and circularly patterned F-shaped slit array subjected to circular polarization illumination are investigated using the finite element method. Different EFDPs appear on two sides in the linearly patterned F-shaped slit array. Reversed EFDPs appear when the handedness of the circular polarization is changed. Large electric fields appear inside or outside the circle in the bent F-shaped slit array depending on the handedness of the circular polarization. These results enrich knowledge on the components of nanophotonic devices for such applications as analyzing circular polarization, focusing SPPs, and generating large electric fields.

References

[1] S. Hayashi and T. Okamoto, "Plasmonics: Visit the past to know the future," *J. Phys. D, Appl. Phys.*, vol. 45, no. 43, pp. 433001-1–433001-24, Oct. 2012.

[2] D. K. Gramotnev and S. I. Bozhevolnyi, "Plasmonics beyond the diffraction limit," *Nature Photon.*, vol. 4, no. 2, pp. 83–91, Jan. 2010.

[3] Z. Xie *et al.*, "Plasmonic nanolithography: A review," *Plasmonics*, vol. 6, no. 3, pp. 565–580, May 2011.

[4] X. G. Luo and T. Ishihara, "Subwavelength photolithography based on surface-plasmon polariton resonance," *Opt. Express*, vol. 12, no. 14, pp. 3055–3065, Jul. 2004.

[5] E. Verhagen, J. A. Dionne, L. (Kobus) Kuipers, H. A. Atwater, and A. Polman, "Near-field visualization of strongly confined surface plasmon polaritons in metal–insulator–metal waveguides," *Nano Lett.*, vol. 8, no. 9, pp. 2925–2929, Jun. 2008.

[6] T. W. Ebbesen, H. J. Lezec, H. F. Ghaemi, T. Thio, and P. A. Wolff, "Extraordinary optical transmission through sub-wavelength hole arrays," *Nature*, vol. 391, no. 6668, pp. 667–669, Feb. 1998.

[7] L. Tang *et al.*, "Nanometre-scale germanium photodetector enhanced by a near-infrared dipole antenna," *Nature Photon.*, vol. 2, no. 4, pp. 226–229, Mar. 2008.

[8] R. A. Pala, J. White, E. Barnard, J. Liu, and M. L. Brongersma, "Design of plasmonic thin-film solar cells with broadband absorption enhancements," *Adv. Mater.*, vol. 21, no. 34, pp. 3504–3509, Jun. 2009.

[9] C. Novo1, A. M. Funston, and P. Mulvaney, "Direct observation of chemical reactions on single gold nanocrystals using surface plasmon spectroscopy," *Nature Nanotechnol.*, vol. 3, no. 10, pp. 598–602, Sep. 2008.

[10] G. Baffou, R. Quidant, and C. Girard, "Heat generation in plasmonic nanostructures: Influence of morphology," *Appl. Phys. Lett.*, vol. 94, no. 15, pp. 153109-1–153109-3, Apr. 2009.

[11] J. A. Schuller, E. S. Barnard, W. H. Cai, Y. C. Jun, J. S. White, and M. L. Brongersma, "Plasmonics for extreme light concentration and manipulation," *Nature Mater.*, vol. 9, no. 3, pp. 193–204, Feb. 2010.

[12] L. Feng, K. A. Tetz, B. Slutsky, V. Lomakin, and Y. Fainman, "Fourier plasmonics: Diffractive focusing of in-plane surface plasmon polariton waves," *Appl. Phys. Lett.*, vol. 91, no. 8, pp. 081101-1–081101-3, Aug. 2007.

[13] Q. Wang, X. Yuan, P. Tan, and D. Zhang, "Phase modulation of surface plasmon polaritons by surface relief dielectric structures," *Opt. Express*, vol. 16, no. 23, pp. 19271–19276, Nov. 2008.

[14] Z. Liu, J. M. Steele, W. Srituravanich, Y. Pikus, C. Sun, and X. Zhang, "Focusing surface plasmons with a plasmonic lens," *Nano Lett.*, vol. 5, no. 9, pp. 1726–1729, Jun. 2005.

[15] Z. Liu, J. M. Steele, H. Lee, and X. Zhang, "Tuning the focus of a plasmonic lens by the incident angle," *Appl. Phys. Lett.*, vol. 88, no. 17, pp. 171108-1–171108-3, Apr. 2006.

[16] H. Caglayan, I. Bulu, and E. Ozbay, "Focusing surface plasmons via changing the incident angle," *J. Appl. Phys.*, vol. 103, no. 5, pp. 053205-1–171108-3, Mar. 2008.

[17] S. Kim, Y. Lim, H. Kim, J. Park, and B. Lee, "Optical beam focusing by a single subwavelength metal slit surrounded by chirped dielectric surface gratings," *Appl. Phys. Lett.*, vol. 92, no. 1, pp. 013103-1–013103-3, Jan. 2008.

[18] H. Shi, C. Wang, C. Du, X. Luo, X. Dong, and H. Gao, "Beam manipulating by metallic nano-slits with variant widths," *Opt. Express*, vol. 13, no. 18, pp. 6815–6820, Sep. 2005.

[19] J. Lin *et al.*, "Polarization-controlled tunable directional coupling of surface plasmon polaritons," *Science*, vol. 340, no. 6130, pp. 331–334, Apr. 2013.

[20] S. Yang, W. Chen, R. L. Nelson, and Q. Zhan, "Miniature circular polarization analyzer with spiral plasmonic lens," *Opt. Lett.*, vol. 34, no. 20, pp. 3047–3049, Oct. 2009.

[21] G. Rui, R. L. Nelson, and Q. Zhan, "Beaming photons with spin and orbital angular momentum via a dipole-coupled plasmonic spiral antenna," *Opt. Express*, vol. 20, no. 17, pp. 18819–18826, Aug. 2012.

[22] G. Rui, W. Chen, D. C. Abeysinghe, R. L. Nelson, and Q. Zhan, "Beaming circularly polarized photons from quantum dots coupled with plasmonic spiral antenna," *Opt. Express*, vol. 20, no. 17, pp. 19297–19304, Aug. 2012.

[23] W. Chen, D. C. Abeysinghe, R. L. Nelson, and Q. Zhan, "Experimental confirmation of miniature spiral plasmonic lens as a circular polarization analyzer," *Nano Lett.*, vol. 10, no. 6, pp. 2075–2079, May 2010.

[24] W. Chen, R. L. Nelson, and Q. Zhan, "Efficient miniature circular polarization analyzer design using hybrid spiral plasmonic lens," *Opt. Lett.*, vol. 37, no. 9, pp. 1442–1444, May 2012.

[25] W. Chen, G. Rui, D. C. Abeysinghe, R. L. Nelson, and Q. Zhan, "Hybrid spiral plasmonic lens: Towards an efficient miniature circular polarization analyzer," *Opt. Express*, vol. 20, no. 24, pp. 26299–26307, Nov. 2012.

[26] H. Kim, J. Park, S.-W. Cho, S.-Y. Lee, M. Kang, and B. Lee, "Synthesis and dynamic switching of surface plasmon vortices with plasmonic vortex lens," *Nano Lett.*, vol. 10, no. 2, pp. 529–536, Jan. 2010.

[27] Y. Gorodetski, A. Niv, V. Kleiner, and E. Hasman, "Observation of the spin-based plasmonic effect in nanoscale structures," *Phys. Rev. Lett.*, vol. 101, no. 4, pp. 043903-1–043903-4, Jul. 2008.